J|A|C|S ARTICLES

Published on Web 10/21/2010

A Paradigm for Blue- or Red-Shifted Absorption of Small Molecules Depending on the Site of π-Extension

Kenneth Hanson,[†] Luke Roskop,[‡] Peter I. Djurovich,[†] Federico Zahariev,[‡] Mark S. Gordon,*[,‡] and Mark E. Thompson*[,†]

Department of Chemistry, University of Southern California, Los Angeles, California 90089, United States, and Department of Chemistry, Iowa State University, Ames, Iowa 50011, United States

Received August 19, 2010; E-mail: mark@si.msg.chem.iastate.edu; met@usc.edu

Abstract: Benzannulation of aromatic molecules is often used to red-shift absorption and emission bands of organic and inorganic, molecular, and polymeric materials; however, in some cases, either red or blue shifts are observed, depending on the site of benzannulation. A series of five platinum(II) complexes of the form (N^N^N)PtCl are reported here that illustrate this phenomenon, where N^N^N represents the tridentate monoanionic ligands 2,5-bis(2-pyridylimino)3,4-diethylpyrrolate (**1**), 1,3-bis(2-pyridylimino)isoindolate (**2**), 1,3-bis(2-pyridylimino)benz(*f*)isoindolate (**3**), 1,3-bis(2-pyridylimino)benz(*e*)isoindolate (**4**), and 1,3-bis(1-isoquinolylimino) isoindolate (**5**). For this series of molecules, either a blue shift (**2** and **3**) or a red shift (**4** and **5**) in absorption and emission maxima, relative to their respective nonbenzannulated compounds, was observed that depends on the site of benzannulation. Experimental data and first principles calculations suggest that a similar HOMO energy level and a destabilized or stabilized LUMO with benzannulation is responsible for the observed trends. A rationale for LUMO stabilization/destabilization is presented using simple molecular orbital theory. This explanation is expanded to describe other molecules with this unusual behavior.

Introduction

The ability to readily tune the optical absorption properties of molecular materials is important for a large number of applications ranging from solar energy conversion to photodynamic therapy.[1] The absorption properties of a molecule or ligand can be controlled by structural modification of the π-conjugated system(s). Two common approaches to tailor the photophysical properties of a molecule, without changing the parent structure, are substitution with donor and/or acceptor groups or extending π-conjugation. The addition of electron-donating and/or electron-withdrawing groups can be used to induce either hypsochromic (blue) or bathochromic (red) shifts in the absorption/emission spectra, by shifting the HOMO or LUMO orbital relative to the unsubstituted compound.[2] On the other hand, extending conjugation, particularly through benzannulation of aromatic rings, is commonly assumed to destabilize the highest occupied molecular orbital (HOMO) and stabilize the lowest unoccupied molecular orbital (LUMO). This decrease in separation between the HOMO and LUMO energies will inevitably lead to red-shifted spectra.[3] An example relevant to this report is the red shift observed when going from benzene to naphthalene to anthracene.[4] However, there are several examples of small molecules that undergo a blue shift in absorption upon benzannulation.[5] This phenomenon was most recently reported for benzannulation of the square planar 1,3-bis(2-pyridylimino)isoindolate platinum chloride, (BPI)PtCl, complex (**2** in Chart 1).[6] Although rationalizations for the unexpected blue shifts have accompanied these reports, a generalized description with predictive capability to explain the effect of benzannulation on absorption has not been given.

To study the effect of benzannulation on the absorption of small molecules, we have focused on a series of 1,3-bis(2-pyridylimino)isoindolate platinum chloride derivatives. These complexes are thermally stable, readily synthesized,[7] easily modified, emissive at room temperature, and have high molar absorptivities.[6]

Herein, we present the synthesis and characterization of a family of (BPI)PtCl derivatives (Chart 1) for which either red or blue shifts are observed when the π-system is extended, for example, λ_{max}(absorption) for complexes **2**, **3**, and **4** are 487, 477, and 529, respectively. The direction of the shift upon

[†] University of Southern California.
[‡] Iowa State University.

(1) (a) *Acc. Chem. Res.* **2009**, *42*, 1859 (special issue). (b) Celli, J. P.; Spring, B. Q.; Rizvi, I.; Evans, C. L.; Samkoe, K. S.; Verma, S.; Pogue, B. W.; Hasan, T. *Chem. Rev.* **2010**, *110*, 2795–2838.
(2) Zollinger, H. *Color Chemistry*, 3rd ed.; Wiley-VCH: Zurich, 2001; p 550.
(3) (a) Griffiths, J. *Colour and Constitution of Organic Molecules*; Academic Press: New York, 1976; p 281. (b) Rogers, J. E.; Nguyen, K. A.; Hufnagle, D. C.; McLean, D. G.; Su, W.; Gossett, K. M.; Burke, A. R.; Vinogradov, S. A.; Pachter, R.; Fleitz, P. A. *J. Phys. Chem. A* **2003**, *107*, 11331–11339.
(4) Turro, N. J.; Ramamurthy, V.; Scaiano, J. C. *Principles of Molecular Photochemistry: An Introduction*; University Science Books: Sausalito, CA, 2009; pp 30−31.
(5) (a) Juris, A.; Barigelletti, F.; Balzani, V.; Belser, P.; Von Zelewsky, A. *Inorg. Chem.* **1985**, *24*, 202–206. (b) Naraso; Nishida, J.-i.; Ando, S.; Yamaguchi, J.; Itaka, K.; Koinuma, H.; Tada, H.; Tokito, S.; Yamashita, Y. *J. Am. Chem. Soc.* **2005**, *127*, 10142–10143. (c) Adachi, M.; Murata, Y. *J. Phys. Chem. A* **1998**, *102*, 841–845. (d) Adachi, M.; Nagao, Y. *Chem. Mater.* **2001**, *13*, 662–669.
(6) Wen, H.-M.; Wu, Y.-H.; Fan, Y.; Zhang, L.-Y.; Chen, C.-N.; Chen, Z.-N. *Inorg. Chem.* **2010**, *49*, 2210–2221.
(7) Siegl, W. O. *J. Org. Chem.* **1977**, *42*, 1872–1878.

Chart 1

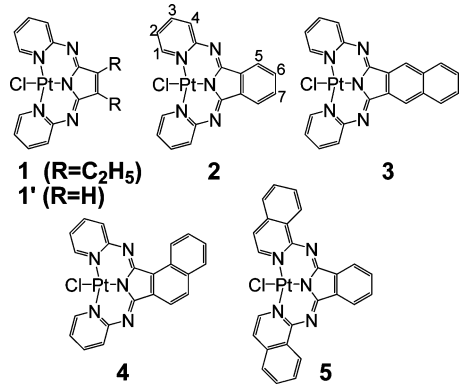

benzannulation is dependent on the site of π-extension. Our experimental and theoretical studies show that the spectral shifts are dependent on the stabilization or destabilization of specific orbitals (e.g., the LUMO) upon benzannulation. In other metal complexes and organic molecules, similar red and blue shifts have been observed as a result of site selective benzannulation. Blue shifts in these compounds have been ascribed to molecular distortions,[8] shifts in total antibonding character,[5c,d] or increased localization of π^* orbitals.[5a] None of these explanations provide a clear understanding of the origin of the shift or how to use it to intentionally tune the transition energies in these materials. The model presented here accurately predicts the direction of the energy shift, due to benzannulation, of a wide range of compounds and gives insight into the origin of the energy shift.

Quantum chemistry calculations are a common tool used to interpret chemical behavior. In many cases, they can provide a rationale that correlates nicely with the experiment, but the use of molecular orbital interpretations is not always justified. The time-dependent density functional theory (TDDFT), which is typically used to calculate the excitations of larger systems, complicates the molecular orbital analysis due to the fact that a given TDDFT excitation could be composed of several molecular-orbital transitions up in energy ("excitations") as well as several transitions down in energy ("de-excitations"). This article introduces a scheme that one can routinely use to determine the validity of an orbital argument based on the Tamm−Dancoff approximation (TDA) to TDDFT, hereinafter referred to as TDA-TDDFT, in which case the molecular excitations are composed of molecular-orbital transitions only up in energy ("excitations").[9] In addition, a dominant molecular-orbital "excitation" may be selected by analyzing the transition amplitudes. Then, further comparisons may be made between the TDA-TDDFT excitation energy and the energy difference corresponding to the dominant transition, for example, HOMO→LUMO if the dominant transition is from the HOMO to the LUMO, as well as with the actual experimental excitation. It will be further shown that the molecules investigated in the current work satisfy the conditions and therefore warrant the use of molecular orbital interpretations.

Experimental Section

General Information. 3-Hexyne, 2-aminopyridine, 1,2-dicyanobenzene, 1-aminoisoquinoline, bromine, copper(I) cyanide, 1,5-cyclooctadiene (Aldrich), 1,2-dicyanonaphthalene, 2,3-dicyanonaphthalene (TCI America), calcium chloride (J.T. Baker), and K_2PtCl_4 (Pressure Chemical Co.) were purchased from the corresponding supplier (in parentheses) and used without further purification for synthesis. $(COD)PtCl_2$,[10] (*E*)-3,4-dibromo-3-hexene,[11] (*E*)- and (*Z*)-3,4-dicyano-3-hexene,[12] 1,3-bis(2-pyridylimino)isoindole,[7] 1,3-bis(2-pyridylimino)isoindolate platinum(II) chloride,[13] and 1,3-bis(2-pyridylimino)benz[*f*]isoindole[14] were synthesized according to literature procedures. All reported NMR spectra were obtained on a Bruker AC-250 MHz FT NMR or a Varian 400 MHz NMR with all shifts given relative to residual solvent signals. Solid probe mass spectrometer (MS) spectra were taken with a Hewlett-Packard MS instrument with electron impact ionization and model 5973 mass selective detector. High resolution mass spectroscopy was performed at the UCR Mass Spectrometry Facility at the University of California, Riverside, CA. Elemental analyses (CHN) were performed at the Microanalysis Laboratory at the University of Illinois, Urbana−Champaign, IL.

2,5-Bis(2-pyridylimino)3,4-diethylpyrrole (BPEP). A mixture of 2 g (14.92 mmol) of (*Z*)-3,4-dicyano-3-hexene, 2.8 g (29.8 mmol) of 2-aminopyridine, and 0.4 g (4 mmol) of $CaCl_2$ in 80 mL of 1-butanol was refluxed under N_2 for 10 days. After removal of 1-butanol under reduced pressure, the remaining residue was separated on a column of silica gel, eluting first with CH_2Cl_2, then a mixture of CH_2Cl_2:ethyl acetate (9:1). The orange fraction was collected and rotary evaporated to dryness to give 187 mg (4%) of a orange solid. ^{1}H NMR (250 MHz, $CDCl_3$, δ): 8.52 (ddd, J = 5, 2, 0.75 Hz, 2H), 7.74 (dd, J = 7.5, 2 Hz, 2H), 7.38 (ddd, J = 7.75, 1.25, 0.75 Hz, 2H), 7.09 (ddd, J = 7.5, 5, 1.25 Hz, 2H), 2.6 (q, J = 7.25 Hz, 4H), 1.24 (t, J = 7.25 Hz, 6H).

2,5-Bis(2-pyridylimino)3,4-diethylpyrrolate platinum(II) Chloride (1). Quantities of 132 mg (0.354 mmol) of $(COD)PtCl_2$ and 100 mg (0.328 mmol) of **BPEP** were suspended in 7 mL of methanol. After the addition of 0.05 mL (0.354 mmol) of NEt_3, the mixture was heated to 60 °C under nitrogen overnight. The mixture was then rotary evaporated to dryness and passed through a plug of silica eluting with CH_2Cl_2. The product was then recrystallized by dissolving the residue in a minimum amount of CH_2Cl_2 and layering with methanol. The precipitate was collected by filtration and washed with methanol to give 85 mg (50%) of thin red needles. MS *m*/*z* (relative intensity): 535.05 (100%), 534.10 (97.5%), 533.10 (82.2%), 536.10 (46.4%), 537.05 (42.5%). ^{1}H NMR (400 MHz, $CDCl_3$, δ): 10.33 (dd, J = 6.4, 1.6 Hz, 2H), 7.90 (td, J = 7.2, 2.0 Hz, 2H), 7.58 (dd, J = 8.0, 1.6 Hz, 2H), 7.02 (td, J = 6.8, 1.6 Hz, 2H), 2.71 (q, J = 7.6 Hz, 4H), 1.27 (t, J = 7.6 Hz, 6H). ^{13}C NMR (100 MHz, $CDCl_3$, δ): 154.3, 152.4, 150.3, 145.3, 137.8, 127.8, 119.7, 18.0, 14.5. HRMS-FAB (*m*/*z*): $[M + H]^+$ calcd for $C_{18}H_{18}N_5PtCl$, 534.0950; found, 534.0944. Anal. Calcd for $C_{18}H_{18}N_5PtCl$: C, 40.42; H, 3.39; N, 13.09. Found: C, 40.70; H, 3.40; N, 12.33.

1,3-Bis(2-pyridylimino)benz(*f*)isoindolate Platinum(II) Chloride (3). Amounts of 0.50 g (1.34 mmol) of $(COD)PtCl_2$ and 0.433 g (1.24 mmol) of **benz(f)BPI** were suspended in 25 mL of methanol. To this solution was added 0.186 mL (1.34 mmol) of triethylamine, and the mixture was heated to 50 °C under nitrogen for 24 h. Upon cooling the reaction mixture to room temperature, precipitate began to form. The precipitate was collected by filtration and washed with water to give 0.554 g (78%) of a pale orange solid. Sample was further purified by sublimation (300 °C, $\sim 10^{-4}$ Torr). MS *m*/*z* (relative intensity): 579.05 (100%), 578.10 (97.4%), 577.10 (79.3%), 580.10 (48.3%), 581.05 (40.0%). ^{1}H NMR (400

(8) Martin, N.; Segura, J. L.; Seoane, C. *J. Mater. Chem.* **1997**, *7*, 1661–1676.
(9) Dreuw, A.; Head-Gordon, M. *Chem. Rev.* **2005**, *105*, 4009–4037, and references therein.
(10) McDermott, J. X.; White, J. F.; Whitesides, G. M. *J. Am. Chem. Soc.* **1976**, *98*, 6521–6528.
(11) Pincock, J. A.; Yates, K. *Can. J. Chem.* **1970**, *48*, 3332–3348.
(12) Fitzgerald, J.; Taylor, W.; Owen, H. *Synthesis* **1991**, *9*, 686–688.
(13) Meder, M.; Galka, C. H.; Gade, L. H. *Monatsh. Chem.* **2005**, *136*, 1693–1706.
(14) Baird, D. M.; Maehlmann, W. P.; Bereman, R. D.; Singh, P. *J. Coord. Chem.* **1997**, *42*, 107–126.

MHz, $CDCl_3$, δ): 10.3 (dd, J = 6.8, 1.6 Hz, 2H), 8.59 (s, 2H), 8.09 (dd, J = 6.0, 3.6 Hz, 2H), 7.95 (td, J = 7.2, 1.6 Hz, 2H), 7.69−7.62 (m, 4H), 7.05 (td, J = 6.8, 1.6 Hz, 2H). HRMS-FAB (m/z): $[M + H]^+$ calcd for $C_{22}H_{14}N_5{}^{196}PtCl$, 580.0660; found, 580.0642. Anal Calcd for $C_{22}H_{14}N_5PtCl$: C, 45.64; H, 2.44; N, 12.10. Found: C, 45.50; H, 2.31; N, 11.69.

1,3-Bis(2-pyridylimino)benz(*e*)isoindole (benz(e)BPI). A solution of 1.0 g (5.6 mmol) of 1,2-dicyanonaphthalene, 1.09 g (11.7 mmol) of 2-aminopyridine, and 0.124 g (1.12 mmol) of $CaCl_2$ in 20 mL of 1-butanol was refluxed under N_2. The reaction was monitored with TLC for the disappearance of 1,2-dicyanonaphthalene. After 20 days of refluxing, the reaction was discontinued even though starting material was still observed. Upon cooling the reaction mixture to room temperature, precipitate began to form. The precipitate was collected by filtration and washed with water. The product was then isolated by column chromatography on silica gel eluting first with CH_2Cl_2, then slow addition of ethylacetate to the eluting solvent. Three fractions were isolated: first was 1,2-dicyanonaphthalene (R_f = 0.6, CH_2Cl_2), second was 1-(2-pyridylimino) isoindol-3-amine (R_f = 0.3, CH_2Cl_2), and finally a yellow fraction containing 1,3-bis(2-pyridylimino)benz(e)isoindole (R_f = 0.1, CH_2Cl_2). The yellow fraction was rotary evaporated to dryness to give 0.320 g (15%) of a yellow solid. ^{1}H NMR (250 MHz, $CDCl_3$, δ): 9.65 (d, J = 8.25, 1H), 8.64 (s, 2H), 8.18−8.04 (m, 2H), 7.97 (d, J = 8.25 Hz, 1H), 7.89−7.45 (m, 6H), 7.20−7.08 (m, 2H).

1,3-Bis(2-pyridylimino)benz(*e*)isoindolate Platinum(II) Chloride (4). Amounts of 0.1 g (0.268 mmol) of $(COD)PtCl_2$ and 0.085 g (0.243 mmol) of **benz(e)BPI** were suspended in 10 mL of methanol. To this solution was added 0.037 mL (0.268 mmol) of triethylamine, and the mixture was heated to 50 °C under nitrogen for 24 h. Upon cooling to room temperature, precipitate began to form. The precipitate was collected by filtration and washed with methanol. The red solid was then dissolved in boiling toluene and then cooled to −40 °C overnight. The red powder was then collected by filtration and washed with MeOH to give 0.062 g (44%) of the desired product. MS m/z (relative intensity): 579.05 (100%), 578.10 (99.8%), 577.10 (82.5%), 580.10 (49.3%), 581.05 (41.9%). ^{1}H NMR (400 MHz, $CDCl_3$, δ): 10.37 (s, 2H), 9.67 (d, J = 8 Hz, 1H), 8.17 (d, J = 8.4 Hz, 1H), 8.09 (d, J = 8.4 Hz, 1H), 7.86−7.60 (m, 7H), 7.08 (d, J = 6.8 Hz, 2H). HRMS-FAB (m/z): $[M + H]^+$ calcd for $C_{22}H_{14}N_5{}^{194}PtCl$, 578.0637; found, 578.0627. Anal. Calcd for $C_{22}H_{14}N_5PtCl$: C, 45.64; H, 2.44; N, 12.10. Found: C, 45.43; H, 2.18; N, 11.67.

1,3-Bis(1-isoquinolylimino)isoindole (BIQI). A mixture of 0.421 g (3.29 mmol) of 1,2-dicyanobenzene, 1 g (6.9 mmol) of 1-aminoisoquinoline, and 0.11 g (1 mmol) of $CaCl_2$ in 20 mL of 1-butanol was refluxed under N_2 for 5 days. Upon cooling the reaction mixture to room temperature, precipitate began to form. The precipitate was collected by filtration and washed with water to give 1.091 g (83%) of a green solid. The sample was used without further purification for the next reaction. ^{1}H NMR (250 MHz, $CDCl_3$, δ): 9.03 (d, J = 8 Hz, 2H), 8.57 (d, J = 5.75 Hz, 2H), 8.28 (dd, J = 5.5, 3 Hz, 2H), 7.88−7.63 (m, 8H), 7.53 (d, J = 5.75 Hz, 2H).

1,3-Bis(1-isoquinolylimino)isoindolate Platinum(II) Chloride (5). Amounts of 0.360 g (0.965 mmol) of $(COD)PtCl_2$ and 0.356 g (0.893 mmol) of **BIQI** were suspended in 20 mL of methanol. To this solution was added 0.134 mL (0.965 mmol) of triethylamine, and the mixture was heated to 50 °C under nitrogen for 24 h. Upon cooling the reaction mixture to room temperature, precipitate began to form. The precipitate was collected by filtration and washed with water to give 0.505 g (90%) of a dark purple solid. Sample was further purified by sublimation (350 °C, ~10^{-4} Torr). Because of the low solubility of the product, NMR data were not obtained. MS m/z (relative intensity): 628.10 (100%), 629.05 (82.4%), 627.00 (61.2%), 630.00 (47.7%), 631.10 (37.9%). HRMS-FAB (m/z): $[M + H]^+$ calcd for $C_{26}H_{16}N_5PtCl$, 628.0794; found, 628.0792. Anal. Calcd for $C_{26}H_{16}N_5PtCl$: C, 49.65; H, 2.56; N, 11.13. Found: C, 49.59; H, 2.41; N, 10.72.

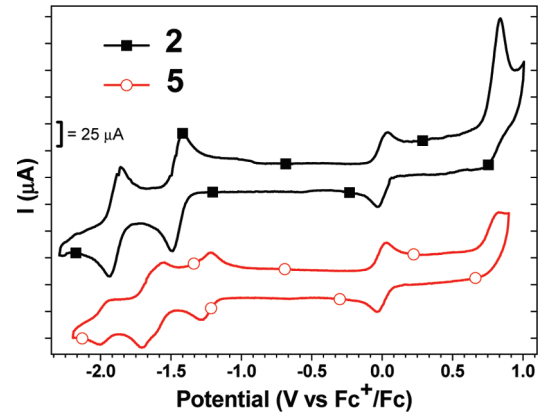

Figure 1. CV of complexes **2** and **5** (150 mV/s). The peaks at 0 V are due to the internal ferrocene reference.

Electrochemical and Photophysical Characterization. All cyclic voltammetry (CV) and differential pulse voltammetry (DPV) were performed using a EG&G Potentiostat/Galvanostat model 283. DMF (VWR), distilled from Type 4A 1/16" molecular sieves (Alfa Aesar), was used as the solvent under inert atmosphere with 0.1 M tetra(*n*-butyl)ammonium hexafluorophosphate (Aldrich) as the supporting electrolyte. A glassy carbon rod, a platinum wire, and a silver wire were used as the working electrode, the counter electrode, and the pseudo reference electrode, respectively. Electrochemical reversibility was determined using CV, while all redox potentials were found using DPV and reported relative to a ferrocenium/ferocene (Fc^+/Fc) redox couple used as an internal standard.[15]

The UV−visible spectra were recorded using an Agilent 8453 UV−visible photo diode array spectrophotometer. Steady-state emission experiments were performed on a Photon Technology International QuantaMaster model C-60 spectrofluorimeter. All lifetime measurements were performed on a IBH Fluorocube lifetime instrument by a time-correlated single-photon counting method using a 405-nm LED excitation source. Quantum efficiency measurements were carried out using a Hamamatsu C9920 system equipped with a xenon lamp, calibrated integrating sphere, and model C10027 photonic multichannel analyzer.

Computational Methods. All properties reported here were determined with first principles electronic structure calculations using the GAMESS electronic structure code.[16] To clearly demonstrate a possible origin of the observed hypsochromic behavior, properties are predicted and analyzed for 2,5-bis(2-pyridylimino)pyrrolate platinum(II) chloride (**1′**) rather than the diethyl substituted 2,5-bis(2-pyridylimino)3,4-diethylpyrrolate platinum(II) chloride structure (**1**). Geometry optimizations for **1′** and **2**-**5** (see Figure 1) were calculated with density functional theory (DFT), employing the hybrid B3LYP functional.[17] Platinum and chlorine are described using small-core model core potentials MCPtzp (triple-ζ + polarization basis set) and MCPdzp (double-ζ +

(15) Gagne, R. R.; Koval, C. A.; Lisensky, G. C. *Inorg. Chem.* **1980**, *19*, 2854–2855.
(16) (a) Schmidt, M. W.; Baldridge, K. K.; Boatz, J. A.; Elbert, S. T.; Gordon, M. S.; Jensen, J. H.; Koseki, S.; Matsunaga, N.; Nguyen, K. A.; Su, S.; Windus, T. L.; Dupuis, M.; Montgomery, J. A. J. *J. Comput. Chem.* **1993**, *14*, 1347–1363. (b) Gordon, M. S.; Schmidt, M. W. *Theories and Applications of Computational Chemistry, the First Forty Years*; Elsevier: Amsterdam, 2005.
(17) (a) Hohenberg, P. *Phys. Rev.* **1964**, *136*, B864–871. (b) Kohn, W.; Sham, L. J. *Phys. Rev.* **1965**, *140*, A1133–1138. (c) Becke, A. D. *J. Chem. Phys.* **1993**, *98*, 5648–5652. (d) Hertwig, R. H.; Koch, W. *Chem. Phys. Lett.* **1997**, *268*, 345–351. (e) Stephens, P. J.; Devlin, F. J.; Chabalowski, C. F.; Frisch, M. J. *J. Phys. Chem.* **1994**, *98*, 11623–11627.

polarization basis set), respectively,[18] whereas all remaining atoms are treated with the all-electron cc-pVDZ basis set.[19] All stationary points were confirmed as minima on the ground-state potential energy surface by calculating and diagonalizing the Hessian (matrix of energy second derivatives). Vertical excitation energies were calculated with time-dependent DFT (TDDFT) using the B3LYP functional. The effects of solvent on the geometry and vertical excitation energies were studied using the Conductor-like Polarizable Continuum Model (CPCM).[20]

The Tamm−Dancoff approximation (TDA)[21] to TDDFT is used here for the purposes of conveniently analyzing the TDDFT excitation energies and validating an orbital analysis. As noted by Dreuw and Head-Gordon,[9] application of the TDA to the DFT linear response equations (TDA-TDDFT) provides an analogue to the simple configuration interaction with single excitations (CIS) method. This is a crucial feature, because an excited state dominated by a single CIS configuration can be approximately characterized using simple orbital arguments. Similar use of an orbital argument is applied here if the TDA-TDDFT method predicts an excited state dominated by a single excitation (e.g., HOMO→LUMO).

Results and Discussion

Synthesis. The ligand precursors for complexes **2**−**5** (BPI, benz(f)BPI, benz(e)BPI, and BIQI, respectively) were synthesized in 15−83% yield using a procedure, metal-ion-catalyzed nucleophilic addition of aromatic amines to dicyano aromatics, developed by Siegl.[7] The precursor for complex **1** (BPEP) was synthesized by bromination of 3-hexyne,[11] followed by substitution with cyanide, photoisomerization,[12] and the nucleophilic addition procedure mentioned above. Photoisomerization of (*E*)-3,4-dicyano-3-hexene was required because all attempts to produce BPEP from the (*E*)-isomer were unsuccessful. The significantly lower yield of BPEP, 4%, may be due to thermal isomerization from (*Z*)-3,4-dicyano-3-hexene to the unreactive (*E*)-isomer.[12]

The complexes **1**−**5** were synthesized in 44−90% yield using $(COD)PtCl_2$ as a metal precursor, rather than the more commonly used $(PhCN)_2PtCl_2$, in accord with the results found by Meder et al.[13] The complexes were characterized by mass spectrometry, elemental analysis, and NMR spectroscopy. Complexes **1**−**5** are soluble in common organic solvents, although increased benzannulation decreases solubility. Differences in solubility can most clearly be observed by the quality of the ^{1}H NMR spectra. Well-resolved ^{195}Pt satellites (J_{Pt-H} = 20.5 Hz) for the pyridyl hydrogens in the meta-position, similar to those reported for $[(2,2';6',2''\text{-terpyridine})PtCl]^+$,[22] can be identified in the highly soluble, diethyl substituted complex **1** (Figure S1). However, due to the low solubility of **5**, we were unable to obtain an acceptable ^{1}H NMR spectrum for this complex. Therefore, the identity and purity of **5** was confirmed by mass spectrometry and elemental analysis.

Electrochemistry. The electrochemical properties of the complexes **1**−**5** were examined using cyclic voltammetry (CV) and differential pulsed voltammetry (DPV). The results of these measurements are listed in Table 1, representative scans for complexes **2** and **5** are shown in Figure 1. All five complexes display irreversible oxidation waves at ∼0.8 V. A small return wave near 0.80 V can also be observed for complexes **1**−**4**; however, full reversibility was not apparent at any of the tested scan rates (50−500 mV/s).

Table 1. Electrochemical Potentials for **1**−**5** Reported in Volts (V) Relative to Fc^+/Fc[a]

complex	$E_{1/2}^{red2}$	$E_{1/2}^{red1}$	E^{ox}	$\Delta E_{1/2}$[b]
1	−1.89	−1.41	0.79	2.20
2	−1.87	−1.44	0.79	2.22
3	−1.95	−1.53	0.80	2.33
4	−1.73	−1.32	0.77	2.09
5[c]	−1.58	−1.23	0.79	2.07

[a] Measurements were performed in an anhydrous solution of 0.1 M NBu_4PF_6 in DMF. [b] $\Delta E_{1/2} = E^{ox} - E_{1/2}^{red1}$. [c] Two additional reversible reduction waves were observed at −1.62 and −1.93 V.

Multiple reversible reduction waves were observed in all five complexes. The complexes with pyridyl groups (**1**−**4**) display two reversible waves. For complexes **1**−**3**, the first reduction peak shifts to more negative values with each successive benzannulation. The trend is counter to the common expectation that the species with the larger π-orbital system will provide a greater stabilization to the negative charge.[23] It is worth noting that the addition of butadiene at the 6,7- and the 5,6-positions of **2** results in a negative shift (**3**; −1.53 V) and a positive shift (**4**; −1.32 V) in reduction potential relative to **2** (−1.44 V).

For complex **5**, a total of four reversible reduction peaks were observed ($E_{1/2}^{red}$ = −1.23, −1.58, −1.62, −1.93 V). The two new reduction waves are likely due to additional reduction sites on the isoquinolyl moieties. Like **4**, complex **5** displays a positive shift in reduction potential relative to **2**, as opposed to the negative shift observed for **3**. This shift in potential leads to a decrease in $\Delta E_{1/2}$ for **5** and **4**, relative to the trend of increasing $\Delta E_{1/2}$ observed in the series **1**−**3** (Table 1).

Electronic Spectroscopy. The absorption spectra for complexes **1**−**5** and their ligand precursors were recorded in CH_2Cl_2 and are shown in Figure 2. The BPI ligand (Figure 2a) displays several absorption bands between 300−425 nm that are assigned to $\pi-\pi^*$ transitions. The spectra for the other four ligands display $\pi-\pi^*$ transitions with a similar vibrational progression (Figure 2a). Upon platination of BPI, the ligand-centered (LC) $\pi-\pi^*$ transitions ($\varepsilon \approx 2 \times 10^4\ M^{-1}\ cm^{-1}$) undergo a red shift, while a new, low energy transition appears between 425−550 nm ($\varepsilon \approx 1.4 \times 10^4\ M^{-1}\ cm^{-1}$). The low energy absorption band is assigned to a combined metal-to-ligand (ML) and intraligand (IL) charge transfer (CT) transition in accord with the prior report by Wen et al.[6] Similarly, distinct LC and ML-ILCT absorption transitions are also observed in the spectra of **1** and **3**−**5** (Figure 2b).

Both the absorption onset and the overall peak position of the ML-ILCT transition in **1**−**3** display a clear trend: a blue shift with each successive benzannulation of the pyrrolate group. This trend is in agreement with the observations of increasing $\Delta E_{1/2}$ in the series, but is counter to the common expectation that expansion of the aromatic π-system will lead to red-shifted absorption.[3] It is also noteworthy that benzannulation of the isoindole ring of **2** results in either a blue shift (in **3**) or a red shift (in **4**) depending on the site of attachment. These observed trends in absorption are in agreement with the change in $\Delta E_{1/2}$ values.

(18) Mori, H.; Ueno-Noto, K.; Osanai, Y.; Noro, T.; Fujiwara, M.; Klobukowski, M.; Miyoshi, E. *Chem. Phys. Lett.* **2009**, *476*, 317–322.
(19) Dunning, T. H., Jr. *J. Chem. Phys.* **1989**, *90*, 1007–1023.
(20) Cossi, M.; Barone, V. *J. Chem. Phys.* **2001**, *115*, 4708–4717.
(21) (a) Fetter, A. L.; Walecka, J. D. *Quantum Theory of Many-Particle Systems*; McGraw-Hill: New York, 1971. (b) Hirata, S.; Head-Gordon, M. *Chem. Phys. Lett.* **1999**, *314*, 291–299. (c) Tamm, I. *J. Phys. (USSR)* **1945**, *9*, 449. (d) Dancoff, S. M. *Phys. Rev.* **1950**, *78*, 382–385.
(22) Cummings, S. D. *Coord. Chem. Rev.* **2009**, *253*, 449–478.
(23) Brooks, J.; Babayan, Y.; Lamansky, S.; Djurovich, P. I.; Tsyba, I.; Bau, R.; Thompson, M. E. *Inorg. Chem.* **2002**, *41*, 3055–3066.

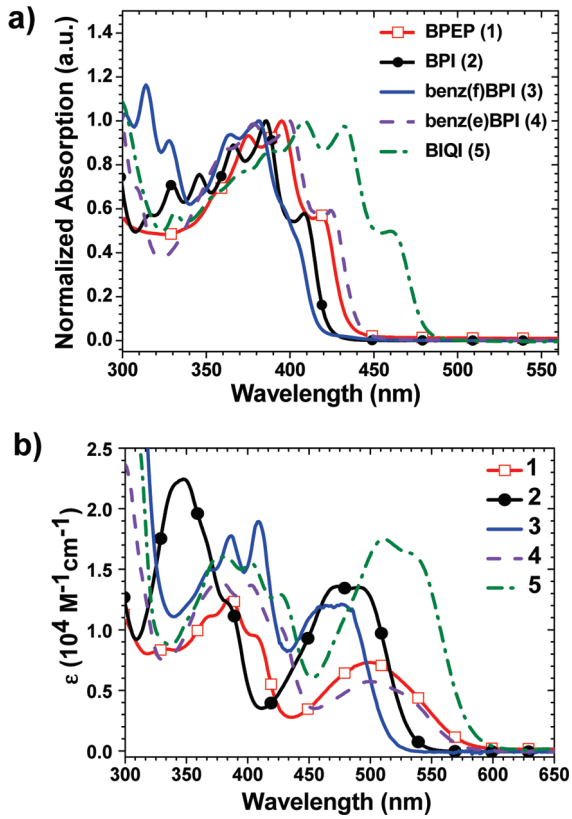

Figure 2. (a) Normalized absorption spectra of free ligands: **BPEP**, **BPI**, **benz(f)BPI**, **benz(e)BPI**, and **BIQI**. The metal complex for each ligand is given in parentheses. (b) Absorption spectra of **1**−**5** at room temperature in CH_2Cl_2.

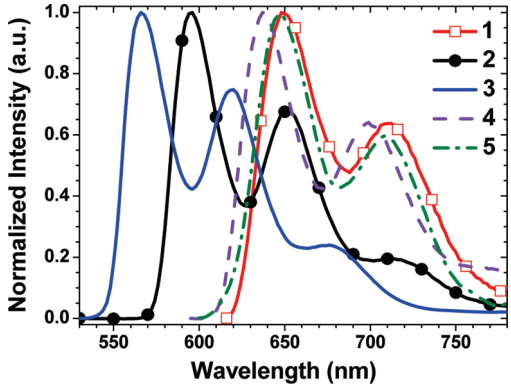

Figure 3. Emission spectra of **1**−**5** in 2-MeTHF at 77 K.

All of the complexes were luminescent in glassy solvent (2-MeTHF) at 77 K (Figure 3), and complexes **2**−**5** were also emissive at room temperature. Emission data for **1**−**5** are summarized in Table 2. The spectra recorded at 77 K display vibronic structure and exhibit long lifetimes (τ = 0.081−20.8 μs), arising from a mixture of $^3[\pi\rightarrow\pi^*(L)]$ ^{3}IL and $^3[5d(Pt)\rightarrow\pi^*(L)]$ ^{3}MLCT triplet excited states as assigned by Wen et al.[6] The quantum yields at room temperature for complexes **2**−**5** varied between 0.3% and 11.5%, whereas **1** was nonemissive and only weakly luminescent even at 77 K. The emission properties of **2** and **3** are in accord with data reported by Wen et al.,[6] although we observe a somewhat higher value for the quantum yield of **2** (Φ = 0.015 vs 0.005) and **3** (Φ = 0.1 vs 0.04) in CH_2Cl_2 (Table 2) presumably due to differences in measurement techniques. The emission energies of **1**−**5** parallel the shifts observed in the absorption spectra that occur with each successive benzannulation. Interestingly, the complexes that show the most red-shifted emission ($\lambda_{max} \approx$ 650 nm) have both the smallest (**1**) and the largest (**5**) π-systems.

Computational Results. The geometry optimized structure of **2** (Figure 4) is in good agreement with the X-ray crystal structure obtained by Meder et al. for the alkyl substituted analogue (6-Me-3-tBuBPI)PtCl (Table 3).[13] The calculated metal−ligand bond lengths differ by less than 0.05 Å, while the chelate bond angles differ by less than 0.5°. The calculations accurately describe an out of the plane distortion (∼10°) of the chlorine atom caused by steric conflict with the ortho-hydrogens (at position 1) of the pyridyl rings (Cl···H = 2.24 Å). Similar bond lengths and angles in the coordination sphere were found in the calculated structures of complexes **1′** and **3**−**5** (Table S1).

From the optimized structures, vertical excitation energies are determined using time-dependent density functional theory (TDDFT). The lowest energy vertical transition for both gas phase and solution (CPCM) calculations (Table 4) show qualitative agreement with the experimental absorption trends (Table 2). The CPCM calculations are in better quantitative agreement with the experimental data than are the gas-phase predictions. As is observed in the experiments for complexes **1**−**3**, a blue shift in absorption is predicted with each successive benzannulation at the pyrrole position. Although complexes **4** and **5** are also benzannulated versions of **2**, they display a red shift in absorption relative to **2**, as opposed to the blue shift observed for **3**. Also listed in Table 4 are the contributions of the HOMO−LUMO configurations to the TDDFT excitation energies. Because the sum of the squares of all such coefficients is unity, it is clear that the HOMO→LUMO contribution dominates these transitions (82−92%). Note also that the TDA-TDDFT vertical excitation energies are in excellent agreement with the TDDFT predictions. This is important: Because the TDA-TDDFT method is essentially equivalent to the CIS wave function approach, the large coefficients in Table 4 provide credence to the use of a HOMO−LUMO argument for qualitatively understanding the observed and predicted trends.[24] Because the HOMO→LUMO transition dominates the excitations that are of interest here, interpretations of the predictions and observations are likely to employ these frontier orbitals.

The Kohn−Sham HOMO and LUMO energies for the ground-state geometries are given in Table 5. The trends in Table 5 correspond closely with those observed in the electrochemistry experiments (Table 1). The calculated HOMO energy levels vary by no more than 0.03 eV, qualitatively agreeing with the near equivalent oxidation potentials for **1**−**5**. The HOMOs of **1′** and **2**−**5** are predominantly localized on the [(pyridylimino)3,4-pyrrolate]PtCl portion of the molecules (Figures 5 and 6), and thus the HOMO energies appear to be dictated by this moiety. In contrast to the invariance in HOMO energies, the energy of the LUMO increases in going from **1′** to **2** to **3**. This trend corresponds to a more negative reduction potential with each successive benzannulation, as is documented in Table 1. On the other hand, the LUMO energies decrease from **2** to **4** to **5** and reflect the values observed for the reduction potentials of each respective complex.

Both the theoretical and the experimental results suggest that the uncharacteristic blue shift in absorption going from **1** to **2** to **3** is due to the destabilization of the LUMO with successive

(24) Of course, unoccupied orbitals are not variationally determined, so arguments based on, for example, a LUMO are only qualitative.

Table 2. Photophysical Properties of Complexes **1**−**5**

		emission at rt[b]					emission at 77 K[c]	
complex	absorbance λ (nm) (ε, $\times 10^4$ M^{-1} cm^{-1})[a]	λ_{max} (nm)	τ (μs)	Φ_{PL}	k_r (10^4 s^{-1})[d]	k_{nr} (10^5 s^{-1})[e]	λ_{max} (nm)	τ (μs)
1	234(2.32), 278(2.14), 385(1.26), 500(0.73)						650	0.081
2	250(5.37), 277(3.51), 348(2.24), 473(1.36), 487(1.35)	641	0.99 (0.97)	0.014 (0.015)	1.4	9.96	595	6.8
3	229(4.16), 300(5.03), 387(1.78), 409(1.89), 467(1.20), 477(1.21)	611	4.5 (3.2)	0.115 (0.098)	2.6	1.97	566	20.8
4	243(2.93), 280(2.95), 376(1.40), 402(1.37), 502(0.57), 529(0.46)	682	0.15	0.003	2.0	66.5	638	1.04
5	245(5.51), 262(5.48), 382(1.61), 403(1.55), 426(1.29), 511(1.75), 536 (1.62)	711	0.051	0.003	5.9	195.5	648	2.0

[a] In CH_2Cl_2. [b] In toluene deaerated with N_2. Data in parentheses recorded in CH_2Cl_2. [c] In 2-MeTHF. [d] $k_r = \Phi/\tau$. [e] $k_{nr} = (1 - \Phi)/\tau$.

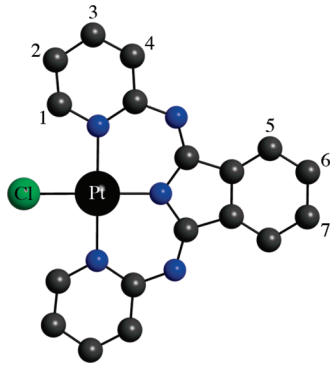

Figure 4. Calculated structure of **2**, with atoms carbon and nitrogen indicated by black and blue spheres respectively. Hydrogen atoms were omitted for clarity.

Table 3. Selected Bond Lengths (Å) and Angles (deg) from DFT Calculations and Reported X-ray Data of **2**

	B3LYP	CPCM/B3LYP	exp[a]
Pt−Cl (Å)	2.36	2.37	2.335(2)
$Pt-N_{pyr}$ (Å)	2.09	2.09	2.049(4)
$Pt-N_{ind}$ (Å)	2.00	2.00	1.966(3)
$Cl-Pt-N_{ind}$ (deg)	171.6	170.5	170.14(12)

[a] From ref 13 (pyr = pyridine, ind = indolate).

Table 4. TDDFT and TDA Vertical Excitation Energies for Gas Phase and CPCM Solvated Complexes

complex	TDDFT vertical excitation energy nm (error)[a]	TDDFT TDA vertical excitation energy nm (error)[a]	square of HOMO→LUMO TDDFT coefficients
1′	541 (−)	566 (−)	0.83
2	519 (32)	508 (21)	0.85
3	498 (21)	488 (11)	0.85
4	564 (35)	553 (24)	0.87
5	575 (39)	564 (28)	0.83
CPCM-**1′**	541 (−)	525 (−)	0.82
CPCM-**2**	489 (2)	478 (9)	0.84
CPCM-**3**	472 (5)	462 (15)	0.86
CPCM-**4**	533 (4)	522 (7)	0.92
CPCM-**5**	540 (4)	527 (11)	0.82

[a] The absolute difference between calculated and experimental transitions, reported in nanometers, is given in parentheses.

expansion of the π-system of the pyrrolate moieties. In a recent report, the destabilization of the LUMO of **3** relative to **2** was rationalized using energetic considerations and bonding/antibonding interactions between the (2-pyridylimino)3,4-pyrrolate and naphthyl portions of the molecules. However, we find that combining a naphthyl fragment with a (2-pyridylimino)3,4-pyrrolate moiety leads to either a destabilization (in **3**) or a stabilization (in **4**) of the LUMO for the two isomers. Clearly the energy of the LUMO in **3** and **4** is not dictated solely by the LUMO energy of naphthalene, and thus the model proffered by Wen et al. does not explain the observed phenomena.[6] Here,

Table 5. HOMO/LUMO Energies and the Kohn−Sham Shifts (HOMO−LUMO Gap) for the Gas Phase and CPCM Solvated Complexes

complex	HOMO energy (eV)	LUMO energy (eV)	Kohn−Sham orbital energy shift (eV)
1′	−5.55	−2.78	2.78
2	−5.55	−2.56	2.99
3	−5.52	−2.45	3.07
4	−5.52	−2.69	2.83
5	−5.52	−2.78	2.75
CPCM-**1′**	−5.74	−2.83	2.91
CPCM-**2**	−5.77	−2.64	3.13
CPCM-**3**	−5.77	−2.56	3.21
CPCM-**4**	−5.74	−2.78	2.96
CPCM-**5**	−5.74	−2.86	2.88

a more quantitative analysis of the LUMO destabilization is presented, using simple molecular orbital theory that relies on both energetic and symmetry considerations of the benzannulation process similar to that used by Uno et al. to explain the observed more negative reduction potentials of *p*-quinones caused by benzannulation.[25]

One can visualize the formation of the frontier molecular orbitals of **2** by combining the valence orbitals of **1′** with those of 1,3-butadiene as illustrated in Figure 5. The HOMO of **1′** consists of contributions from the respective p- and d-orbitals of the chloride and platinum atoms, as well as from the π-system of the pyridyl and imino-pyrrolate portions of the ligand. There is minimal HOMO density at the site of benzannulation of **1′** by 1,3-butadiene; thus no orbital mixing is observed and the HOMO energy remains unchanged in **2**. The LUMO of **1′** is localized primarily on the π-system of the ligand with only a small contribution from the d-orbital on the Pt atom. If one ignores the out of plane distortion of the chloride atom, **1′** can be idealized as having C_{2v} symmetry. In this point group, the LUMO of **1′** can be considered to have a_2 symmetry. The frontier orbitals of *cis*-1,3-butadiene also fall under the C_{2v} point group with the HOMO and LUMO designated as a_2 and b_1, respectively. The LUMO of 1,3-butadiene (b_1) does not have the appropriate symmetry to mix with the LUMO of **1′** (a_2). However, both the HOMO of 1,3-butadiene and the LUMO of **1′** have the same a_2 symmetry, so they can combine to create an occupied bonding MO (not shown) and an unoccupied antibonding orbital (LUMO of **2**) with the addition of a new nodal plane at the site of attachment. The favorable orbital symmetry enables the HOMO of 1,3-butadiene to act as an effective electron-donating group to the LUMO of **1′**. The net effect of these interactions is an unaltered HOMO and a destabilized LUMO, resulting in the blue-shifted absorption upon benzannulation of **1′**. Likewise, a similar combination between the frontier orbitals of **2** and 1,3-butadiene leads to an

(25) Uno, B.; Kano, K.; Konse, T.; Kubota, T.; Matsuzaki, S.; Kuboyama, A. *Chem. Pharm. Bull.* **1985**, *33*, 5155–5166.

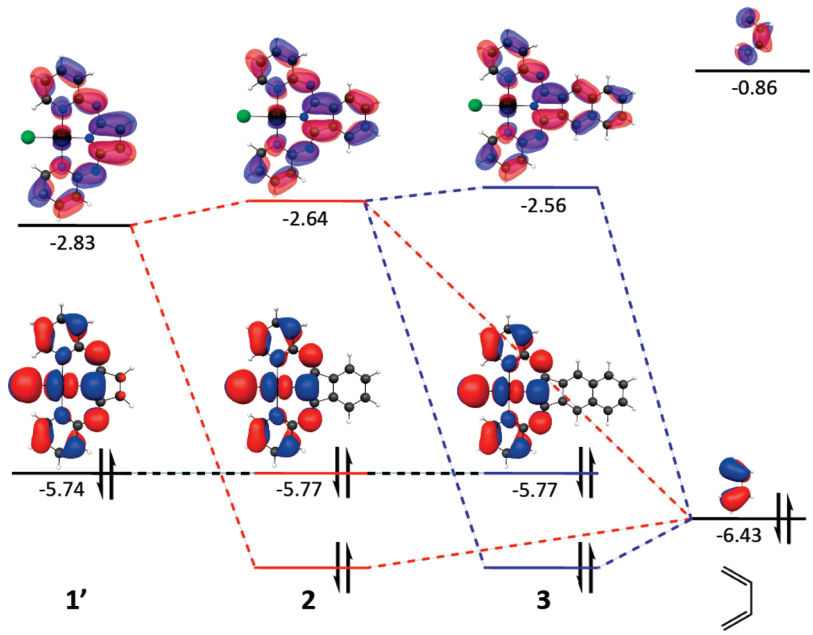

Figure 5. Qualitative orbital diagram of the valence orbitals for complexes **1′**, **2**, and **3**. The HOMO (bottom, solid) and LUMO (top, transparent) surfaces are displayed as viewed above the π-symmetric orbitals, with opposite phases above and below the plane of the molecule.

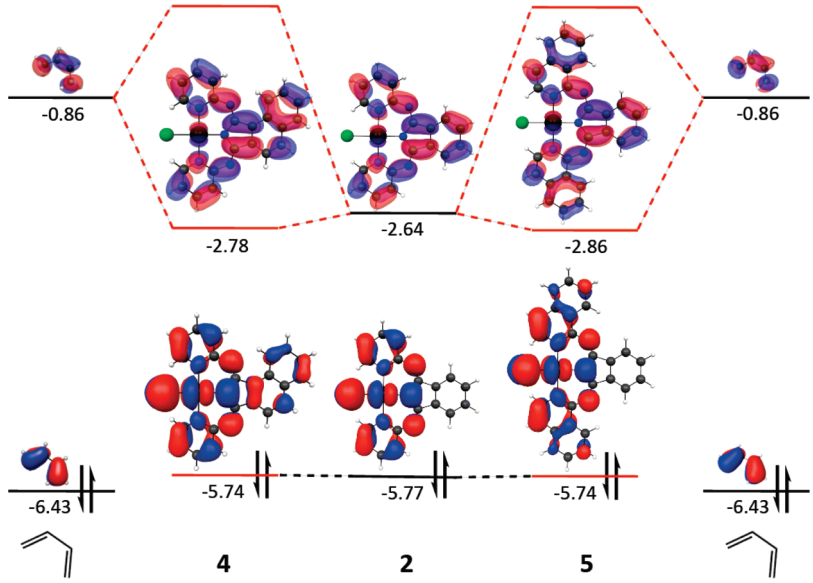

Figure 6. Qualitative orbital diagram of the valence orbitals for complexes **2**, **4**, and **5**.

unaltered HOMO and a destabilized LUMO as seen in **3** (Figure 5). Even when the geometry distorts somewhat from the idealized C_{2v} symmetry, the nodal behavior of the orbitals at the site of butadiene addition can be used to make the same qualitative arguments. This is expanded upon in the following paragraphs.

The arguments regarding the symmetry of interacting orbitals can also be used to interpret the effects of benzannulation at other positions of **2**. The stabilizing effect on the LUMO when **2** is benzannulated at either the 5,6- or the 3,4-positions (to form **4** and **5**, respectively) is illustrated in Figure 6. The orbitals of **2** can be characterized by the presence or absence of a bisecting nodal plane at the site of benzannulation. The absence of a perpendicular bisecting nodal plane at either of the relevant positions of the LUMO of **2** favors a cooperative interaction with the LUMO of 1,3-butadiene that leads to a bonding/antibonding pair of MOs, whereas interactions with the HOMO of 1,3-butadiene are disfavored. The end result is a stabilized LUMO in both **4** and **5**. Analogous symmetry considerations predict that benzannulation at either the 1,2- or the 2,3- position of **2** should stabilize and destabilize the LUMO, respectively, an outcome that is supported by calculation (Figure S7).

The unexpected destabilization of the LUMO, and corresponding increase in reduction potential, exhibited by **2** and **3** has been observed in other molecules that have their π-systems extended with either 1,3-butadiene or ethene. These examples include tetracyanoquinones (TCNQ),[8] indoanilines,[5c] anhydrides,[5d] Ru(polypyridyl)$_3$,[5a] complexes and phthalocyanines,[26] as well as in simple polycyclic aromatic hydrocarbons.[27] The destabilization of the LUMO has been attributed to either molecular distortions (in TCNQ),[8] an increase in the total

Chart 2

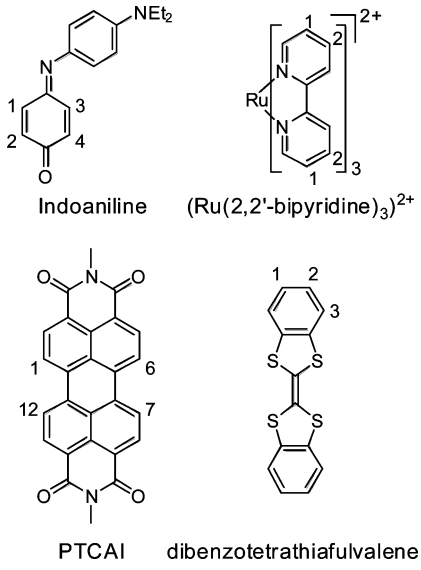

antibonding character of the orbital (in indoanilines and anhydrides),[5c,d] or an increased localization of the π^* orbital (in Ru(polypyridyl) complexes).[5a] The molecular orbital model presented here can be successfully applied to all of these molecular systems to rationalize the origin of the unusual LUMO destabilization by the same sort of orbital mixing approach described for compounds **2** and **3**.

As with complexes **1**−**3**, benzannulation in several of these systems leads to destabilization of the LUMO, which manifests itself in both increased reduction potentials and blue-shifts in the lowest energy absorption transitions. A necessary requirement to observe the blue-shift is for the HOMO energy to be either stabilized or remain relatively unchanged upon benzannulation. This condition is met when the HOMO is electronically isolated from the site of benzannulation. For example, indoaniline dyes (Chart 2) have a HOMO localized on the *p*-diaminophenyl fragment and a LUMO localized on the *p*-quinoaniline moiety.[5c] The low energy charge transfer absorption bands in these molecules undergo a progressive shift from 596 nm to 589 nm to 558 nm when the 1,2- and 3,4-positions of the quinoaniline fragment are successively benzannulated. The shift to higher energy is attributed to an increase in LUMO energy that accompanies each benzannulation, while the HOMO energy remains relatively unchanged. Likewise, benzannulation at the 1,2-positions of (Ru(2,2′-bipyridine)$_3$ leads to a 60 nm blue shift in the lowest energy absorption band.[5a] This shift is the result of LUMO destabilization as the reduction potential is shifted by 0.16 V ($E_{1/2} = -1.51$ V vs SCE in Ru(2,2′-biisoquinoline)$_3$ vs −1.35 V in Ru(bpy)$_3$). While the HOMO energy is stabilized by 0.14 V, the change relative to the LUMO is smaller, and thus a blue shift is observed.

Although the discussion so far has focused on molecules that exhibit a blue-shifted absorption upon benzannulation, there are several examples where LUMO destabilization occurs and red-shifted absorption is observed. For example, theoretical investigations of porphyrins have shown that these molecules exhibit a destabilized LUMO upon benzanulation.[3b,26] The amount of LUMO destabilization is small relative to the HOMO destabilization; thus an overall red shift is observed. Similarly, DFT calculations by Nguyen and Pachter show that the LUMOs of tetra-azaporphyrins are destabilized when benzannulated to form phthalocyanines.[26]

Thus far, the orbital symmetry analysis used to explain the destabilization of the LUMO has been limited to benzannulation with 1,3-butadiene; however, the same principles can also be applied to molecules whose π-systems are expanded by the addition of ethene. For example, Adachi, et al. found that benzannulation with ethene at the 1,12- and 6,7-positions of 3,4,9,10-perylenetetracarboxylic dianhydride diimide (PTCAI, Chart 2) to give coronenetetracarboxylic dianhydride diimide (CTCAI) resulted in an increase in the LUMO energy.[5d] The LUMO of PTCAI (b_{2g} symmetry) has an in-phase pair of orbitals at the 1,12- and 6,7-positions that can combine with the π-symmetric HOMO, but not the π-antisymmetric LUMO, of ethene in a fashion similar to that shown in Figure 5 for **2** (see Figure S8). The favorable interaction between the LUMO of PTCAI and the HOMO of ethene will consequently destabilize the LUMO of PTCAI. The upward shift in the LUMO energy that occurs upon ethene addition to PTCAI has a parallel in the change in the reduction potentials found for perylene ($E_{1/2} = -1.64$ V vs SCE) versus corannulene ($E_{1/2} = -2.03$ V vs SCE).[27]

A slightly more complex situation alters the HOMO of PTCAI when the π-system is expanded to form CTCAI. The HOMO of PTCAI is stabilized by a bonding/antibonding interaction between the π-antisymmetric LUMO of ethene and the out-of-phase pair of orbitals at the 1,12- and 6,7-positions in the HOMO (a_u) of PTCAI (Figure S8). On the other hand, the HOMO−4 (b_{1u}) of PTCAI has an in-phase pair of orbitals at the same positions, and, as a result, this orbital is strongly destabilized by an antibonding interaction with the π-symmetric HOMO of ethene. The energy of the HOMO−4 of PTCAI is so destabilized that it becomes the HOMO of CTCAI. The result of these interactions is that the HOMO (LUMO) of CTCAI is stabilized (destabilized) relative to the parent PTCAI. Thus, a net blue shift in the lowest energy transition from 526 nm in PTCAI[28] to 511 nm in CTCAI is observed.[29]

The arguments given above to explain the stabilization/destabilization of the LUMO energies upon benzannulation can also be used to rationalize related shifts in HOMO energies in molecules that serve as electron donors. For example, tetrathiafulvalene (TTF, $E_{1/2} = 0.35$ V vs SCE) becomes more difficult to oxidize upon benzannulation to form dibenzotetrathiafulvalene ($E_{1/2} = 0.60$ V vs SCE).[5b] Benzannulation of dibenzotetrathiafulvalene results in either an increase (1,2-position; $E_{1/2} = 0.72$ V vs SCE)[5b] or a decrease (2,3-position; $E_{1/2} = 0.52$ V vs SCE)[30] in oxidation potential depending on the orbital symmetry at the site of butadiene addition (Figure 7). The atypical HOMO stabilization upon benzannulation again results in a blue-shifted absorption from 516 nm in dibenzotetrathiafulvalene to 502 nm in the linear dinaphthotetrathiafulvalene.

Conclusion

A series of (BPI)PtCl derivatives with varying degrees of benzannulation have been prepared, and their properties have

(26) Nguyen, K. A.; Pachter, R. *J. Chem. Phys.* **2001**, *114*, 10757–10767.
(27) Jensen, B. S.; Parker, V. D. *J. Am. Chem. Soc.* **1975**, *97*, 5211.
(28) Adachi, M.; Murata, Y.; Nakamura, S. *J. Phys. Chem.* **1995**, *99*, 14240–14246.
(29) Rohr, U.; Schlichting, P.; Bohm, A.; Gross, M.; Meerholz, K.; Brauchle, C.; Mullen, K. *Angew. Chem., Int. Ed.* **1998**, *37*, 1434–1437.
(30) Schukat, G.; Fanghanel, E. *J. Prakt. Chem.* **1979**, *321*, 675–679.

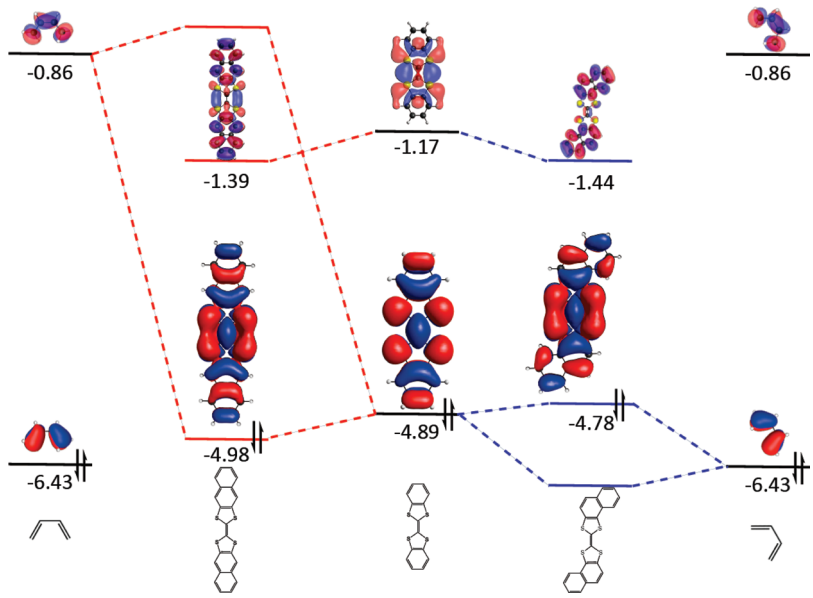

Figure 7. Qualitative orbital diagram for benzannulated dibenzotetrathiafulvalene complexes.

been characterized. It is observed that the lowest energy absorption/emission transitions undergo a red or blue shift depending on the site of benzannulation. Experimental data and first principles calculations suggest that the observed trends are caused by an unvaried HOMO energy level and a destabilized or stabilized LUMO with benzannulation. A rationale for the stabilization/destabilization of the LUMO is presented using simple molecular orbital theory. The molecular orbital model presented here can also be successfully applied to indoaniline dyes, $(Ru(2,2'\text{-bipyridine})_3)^{2+}$, 3,4,9,10-perylenetetracarboxylic dianhydride diimide, and dibenzotetrathiafulvalene, to explain unusual blue shifts in absorption with benzannulation.

Although the focus in this Article has been to describe blue shifts in absorption upon benzannulation, the ability to selectively tune HOMO and LUMO energy levels while extending conjugation may be particularly useful in organic electronics. This concept is exemplified in TTF systems mentioned above where the increased field-effect transistor performance of dinaphthotetrathiafulvalene over dibenzotetrathiafulvalene has been attributed to the more extended π-system and its effects on film morphology.[5b] This orbital analysis can also readily be applied to design new solar cell and charge transfer materials where molecular organization and the ability to tune the energy of the frontier orbitals of donor and acceptor molecules is of the utmost importance.

This article has also introduced a method that one can routinely use to determine the validity of a molecular orbital-based argument to explain the observed electronic properties of a given molecule or series of molecules. The method presented here relies on time-dependent DFT and related theoretical methods and their correlation with experimental data. In particular, this approach is based on the Tamm−Dancoff approximation (TDA) to TDDFT. The orbitals predominantly involved in this transition are determined from the coefficients of the corresponding configurations for the lowest energy excitation. If the TDA-TDDFT transition matches that derived by TDDFT, and if the energy of the transition correlates with experimental absorption energies, the application of an orbital argument is valid. It was demonstrated that the molecules investigated in the current work satisfy these conditions and therefore warrant the use of molecular orbital interpretations.

Acknowledgment. K.H., P.I.D., and M.E.T. thank Universal Display Corp. and the Department of Energy for their financial support of this work. L.R., F.Z., and M.S.G. are grateful for the support of the Air Force Office of Scientific Research.

Supporting Information Available: ^{1}H NMR of **1**−**4**, room temperature emission spectra of **2**−**5**, the orbital diagram for PTCAI, and the products of benzanulation at the 2,3-position and the 1,2-position of **2**. This material is available free of charge via the Internet at http://pubs.acs.org.

JA1075162